Int J Adv Manuf Technol (2009) 44:906–920
DOI 10.1007/s00170-008-1919-1

ORIGINAL ARTICLE

Applications of integrated motion controllers for precise CNC machines

Syh-Shiuh Yeh · Zheng-Hong Tsai · Pau-Lo Hsu

Received: 15 May 2008 / Accepted: 23 December 2008 / Published online: 6 February 2009

Abstract The error resources of precise motion control systems are basically categorized into linear and nonlinear effects. To realize the precise motion of industrial computer numerical control (CNC) machines, this paper presents an integrated motion control structure with modular algorithms, including both the linear control and the nonlinear compensation. In the linear control design, this study applies three algorithms: (1) feedforward control to address the tracking errors, (2) cross-coupled control to reduce the contouring errors, and (3) digital disturbance observer to lessen the effects of modeling errors and disturbances in real applications. The results indicate that the linear motion controller achieves greatly improved accuracy in both tracking and contouring by reducing the servo lags and mismatched dynamics of the different axes. However, the adverse effect due to friction still exists and cannot be eliminated by applying the linear motion controller only. This study further integrates the nonlinear compensator and develops friction estimation and compensation rules for CNC machines. The digital signal processors are suitable to implement all the developed linear and nonlinear algorithms, and the present controllers have been successfully applied to industrial CNC machines. Experimental results on a vertical machining center indicate that, under different feed rates, the CNC machine with the integrated motion controller significantly reduces the maximum contouring error by 135% on average.

Keywords Motion control · Friction compensation · CNC machine

S.-S. Yeh (✉)
Department of Mechanical Engineering,
National Taipei University of Technology,
Taipei 10608, Taiwan
e-mail: ssyeh@ntut.edu.tw

Z.-H. Tsai · P.-L. Hsu
Department of Electrical and Control Engineering,
National Chiao Tung University,
Hsinchu 300, Taiwan

1 Introduction

Microprocessors have rapidly developed in the past two decades with increasing computation speeds and decreasing costs; hence, they have been extensively applied to the motion control design for computer numerical control (CNC) machines to realize higher precision motion at higher speeds in modern manufacturing industries. In addition to the dynamic effects of the mechanical structure, the dynamic systems including the improper control loop gains, incompatible dynamic responses among axes, servo lags, loading, and external disturbances contribute to the motion error that can be overcome by applying a suitable control design [1]. In addition to the abovementioned motion errors in linear problems, the nonlinear friction also plays an important role in precise motion control. If merely a linear design is adopted in motion controller realization, the desirable motion performance cannot be achieved. Hence, in this paper, we implement the integrated motion control design that includes both the linear motion controller and the nonlinear compensator in an industrial CNC machine through a high-performance digital signal processor (DSP) microprocessor and study the precision and robustness of the motion system of the CNC machine. This study shows that the precision and robustness of CNC machines can be greatly improved using the integrated motion controller.

Generally, feedforward controllers are effective in improving the tracking accuracy. Their design concept

basically applies the pole-zero cancellation to shape the dynamic characteristics of servo systems. However, for systems with unstable and lightly damped zeros, they cannot be cancelled directly [2]. The zero-phase error tracking control (ZPETC) was proposed by Tomizuka [3]. It should be noted that since the ZPETC is a model-based design, the tracking ability is sensitive to all modeling errors, plant parameter variations, and external disturbances—friction, inertia, cutting force, measurement noise, and torque ripple. In other words, system uncertainty and disturbances easily affect the tracking accuracy; therefore, another auxiliary control design is desired for the current feedforward controller design.

Moreover, Koren and Lo [1] proposed the variable-gain cross-coupled control (CCC) that significantly improves the contouring accuracy. Hsu and Houng [4] suggested the concept of integrated control that includes both the ZPETC and the CCC to improve both the tracking performance and contouring accuracy simultaneously. Furthermore, Yeh and Hsu [5] recommended the method of estimation of the contouring error vector for multi-axis CCC-controlled systems. Shih et al. [6] proposed a new structure for the CCC for precise tracking in a microcomputer-controlled dual-axis positioning system by reprogramming the reference position command subroutine. Chen et al. [7] suggested a contouring controller based on the polar coordinates of motion for improving the contouring accuracy of biaxial systems. The contouring control problem is thus transformed into a stabilization problem by considering the contouring error as a state variable.

Recently, Lo [8] proposed an approach that transforms the coordinate to obtain the moving basis to form a feedback controller for three-axis motion systems. Chiu and Tomizuka [9] recommended a task-coordinated approach by considering all axes as first-order loops to obtain the feedback and feedforward control loops separately. However, Lo's approach cannot be easily applied to more than three axes. Moreover, as this approach does not have a feedforward control loop, its tracking accuracy can be further improved. On the other hand, the performance of the first-order design with an unreliable plant model by Chiu and Tomizuka [9] is inherently limited. Yeh and Hsu [10] further proposed the independent control design of a control structure that consists of a feedback control, feedforward control, and the CCC. Chen et al. [11] suggested the position command shaping control based on the hybrid control of the feedforward controller and CCC to improve the tracking performance and reduce the contouring errors in multi-axis motion systems. However, the application of some advanced control structures significantly improves both the tracking and contouring performances of multi-axis motion systems; the performances of motion systems are still limited by some adverse effects caused by modeling errors, uncertainties, external disturbances, and nonlinear friction.

In real applications, system uncertainty and external disturbance affect the robustness of precise motion systems. Ohishi et al. [12] proposed the structure of a disturbance observer (DOB) to suppress the disturbances and increase the robustness of systems. Umeno and Hori [13] further recommended a DOB that includes all the system uncertainties, external disturbances, friction, and changes in loading as an unknown disturbance torque. The DOB estimation and compensation eliminate the external disturbances in the low frequency range; furthermore, the noise effects in higher frequencies are also effectively suppressed. Moreover, the design of a digital disturbance observer (DDOB) was developed in the discrete time domain in practice [14, 15] to compensate the undesired nonlinearity and external load disturbance of motion systems.

In addition, friction is a dominant factor that limits the motion precision in CNC. However, the friction in CNC is usually neglected or addressed by general linear controllers because of its highly nonlinear properties. The approach of compensating for friction errors is based on the estimated friction that includes the magnitude and location at which it occurs with a simple friction model [16, 17]. However, in practice, it is not easy for CNC to predict precisely the location at which significant friction will occur. Moreover, since there is a discontinuity evident near the zero velocity, this inadequate compensation may easily result in an oscillatory system [18–20]. In this paper, motion error is eliminated to some extent by applying linear controllers such as the feedforward controllers, feedback controllers, and DDOBs. The identification of a friction model is then achieved by constructing a relationship between the velocity and the friction torque. Frictional compensation is subsequently applied to eliminate the friction phenomenon.

In this study, an integrated motion control structure that combines all the linear controllers with the nonlinear friction compensators is applied to a vertical machining center to achieve both good tracking and contouring accuracy in real applications. In the integrated control structure, the feedforward control with zero-phase error (ZPETC) improves the tracking ability; the CCC improves the contouring accuracy; the DDOB suppresses the uncertainties, modeling errors, and external disturbances; and the nonlinear friction compensator (NC) eliminates the friction phenomenon. The integrated motion control structure is implemented on a vertical machining center through a TI TMS320C32 floating-point DSP microprocessor. Experimental results show that the maximum contouring error is reduced by 135% on average under different feed rates. Moreover, measurements of the maximum contouring error using a double ball bar (DBB) also show a reduction by 120% by applying the integrated control structure.

2 Design of the linear controllers

To cope with the motion error caused by servo lag, mismatched dynamics among the axes, and external disturbances, this paper adopts three controllers: (1) feedforward controller, (2) the CCC, and (3) the DDOB to address effectively the problems of tracking error, contouring error, and disturbance effects, respectively.

2.1 Design of the feedforward controller

To provide a good tracking ability in the position loop of servo systems, a suitable feedforward controller is placed in front of the position loop to cancel all the poles and stable zeros. However, to deal with unstable zeros, the design of the ZPETC compensates for the unstable and lightly damped zeros to achieve a zero-phase error and a unity DC gain in the frequency response. The ZPETC has been proven to be effective in real applications in reducing the tracking error [3].

The general two degrees of freedom (2DOF) controller design for a tracking control system is shown in Fig. 1. The unstable and lightly damped zeros in the position feedback loop are called the unacceptable zeros, while the stable and well-damped zeros in the position feedback loop are called the acceptable zeros. The position feedback loop transfer function $T(z^{-1})$ is represented as follows:

$$T(z^{-1}) = \frac{Y(z^{-1})}{U(z^{-1})} = \frac{z^{-d}B(z^{-1})}{A(z^{-1})} = \frac{z^{-d}\hat{B}(z^{-1})}{\hat{A}(z^{-1})} = \frac{z^{-d}B_{\mathrm{a}}(z^{-1})B_{\mathrm{u}}(z^{-1})}{\hat{A}(z^{-1})} \quad (1)$$

where

$$A(z^{-1}) = 1 + a_1 z^{-1} + a_2 z^{-2} + \cdots + a_n z^{-n}$$

$$B(z^{-1}) = b_0 + b_1 z^{-1} + b_2 z^{-2} + \cdots + b_m z^{-m}$$

$$\hat{A}(z^{-1}) = \hat{a}_0 + \hat{a}_1 z^{-1} + \hat{a}_2 z^{-2} + \cdots + \hat{a}_n z^{-n}$$

$$\hat{B}(z^{-1}) = 1 + \hat{b}_1 z^{-1} + \hat{b}_2 z^{-2} + \cdots + \hat{b}_m z^{-m}$$

$$B_{\mathrm{a}}(z^{-1}) = 1 + b_1^{\mathrm{a}} z^{-1} + b_2^{\mathrm{a}} z^{-2} + \cdots + b_q^{\mathrm{a}} z^{-q} \text{ (polynomials with acceptable zeros)}$$

$$B_{\mathrm{u}}(z^{-1}) = 1 + b_1^{\mathrm{u}} z^{-1} + b_2^{\mathrm{u}} z^{-2} + \cdots + b_p^{\mathrm{u}} z^{-p} \text{ (polynomials with unacceptable zeros)}$$

The ZPETC is originally designed to achieve zero-phase error with a unity DC gain [3]. To improve the frequency response of the tracking control system, as shown in Fig. 1, a feedforward controller $Z_p(z^{-1})$ with a digital prefilter (DPF) is designed as

$$Z_p(z^{-1}) = \mathrm{DPF}(z^{-1}) \cdot \frac{z^d \hat{A}(z^{-1})}{B_{\mathrm{a}}(z^{-1})} \quad (2)$$

Thus, the transfer function $R(z^{-1})$ of the whole control system becomes

$$R(z^{-1}) = \frac{Y(z^{-1})}{Y_m(z^{-1})} = Z_p(z^{-1}) \cdot T(z^{-1}) = \mathrm{DPF}(z^{-1}) \cdot B_{\mathrm{u}}(z^{-1}) \quad (3)$$

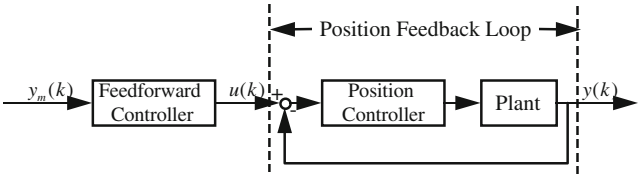

Fig. 1 2DOF tracking control system

where the tracking error caused by the polynomial $B_{\mathrm{u}}(z^{-1})$ is expected to be further compensated for by applying the digital prefilter $\mathrm{DPF}(z^{-1})$. To compensate for the undesirable polynomial $B_u(z^{-1})$, the digital prefilter $\mathrm{DPF}(z^{-1})$ can be designed as

$$\mathrm{DPF}(z^{-1}) = \frac{B_{\mathrm{u}}(z)}{B_{\mathrm{u}}(1)^2} \quad (4)$$

By substituting Eq. 4 into Eq. 3, the control system transfer function $R(z^{-1})$ becomes

$$R(z^{-1}) = \mathrm{DPF}(z^{-1}) \cdot B_{\mathrm{u}}(z^{-1}) = \left(\frac{B_{\mathrm{u}}(z)B_{\mathrm{u}}(z^{-1})}{B_{\mathrm{u}}(1)^2}\right) = \left(\sum_{i=0}^{P} \gamma_i \cdot (z^i + z^{-i})\right) \quad (5)$$

where γ_i is the coefficient of the polynomial $\left(\frac{B_{\mathrm{u}}(z)B_{\mathrm{u}}(z^{-1})}{B_{\mathrm{u}}(1)^2}\right)$ corresponding to the order z^i and P denotes the number of

unacceptable zeros in the position feedback loop. Thus, the ZPETC feedforward controller is obtained as follows:

$$Z_p(z^{-1}) = \left(\frac{B_u(z)}{B_u(1)^2}\right) \cdot \left(\frac{z^d \hat{A}(z^{-1})}{B_a(z^{-1})}\right) \tag{6}$$

2.2 Design of the CCC

To eliminate the contouring error, the CCC is designed to coordinate the position error among the axes and compensate for each axis according to its geometric components. The block diagram of a two-axis cross-coupled motion-control system is shown in Fig. 2. This CCC motion-control system has three degrees of freedom, two position loop controllers (K_{px}, K_{py}), and a compensator C.

The cross-coupling gains (C_x, C_y) are directly determined according to the contouring commands [1]. For linear contours, the gains (C_x, C_y) are determined as follows:

$$C_x = \sin\theta \tag{7}$$

$$C_y = \cos\theta \tag{8}$$

where θ is the inclination angle of a linear contour with respect to the X-axis. For circular contours, the variable gains (C_x, C_y) are determined as

$$C_x = \sin\theta - \frac{E_x}{2R} \tag{9}$$

$$C_y = \cos\theta + \frac{E_y}{2R} \tag{10}$$

where R is the circular contour radius; (E_x, E_y)are the X- and Y-axes error signals, respectively; and θ is the circular contour traversal angle input command. As shown in Eqs. 7, 8, 9, and 10, the cross-coupling gains are determined by the orientation in linear motions and the traversal angle in circular motions. Therefore, the CCC control system that combines the CCC controller and the plant is a parameter-varying system. If the axial errors are considerably smaller than the circular motion circle radius [1], the cross-coupling gains (C_x, C_y) in Eqs. 7, 8, 9, and 10 can be reasonably confined within the range of [−1, 1] in the CCC design. In this study, the concept of the contouring error transfer function (CETF) is applied to design the compensator C.

In uncoupled systems, C=0 and ε_o is denoted as the uncoupled motion-control system contouring error, where the subscript "o" indicates an open cross-coupling connection. The contouring error of the uncoupled system is derived as follows [10]:

$$\varepsilon_o = \frac{1}{(1+P_2K_{py})(1+P_1K_{px})} \left[-(1+P_2K_{py})C_x(1+P_1K_{px})C_y\right][X_r\ Y_r\ ] \tag{11}$$

ε_c is defined as the contouring error of a coupled motion-control system, where the subscript "c" refers to a "coupled system." As shown in Fig. 2, if $C\neq 0$, the contouring error of the coupled motion-control system ε_c is derived as [10]

$$\varepsilon_c = \frac{1}{\left[(1+P_2K_{py})(1+P_1K_{px}) + (1+P_1K_{px})CC_yC_yP_2 + (1+P_2K_{py})CC_xC_xP_1\right]} \cdot \left[-(1+P_2K_{py})C_x(1+P_1K_{px})C_y\right][X_r\ Y_r\ ] \tag{12}$$

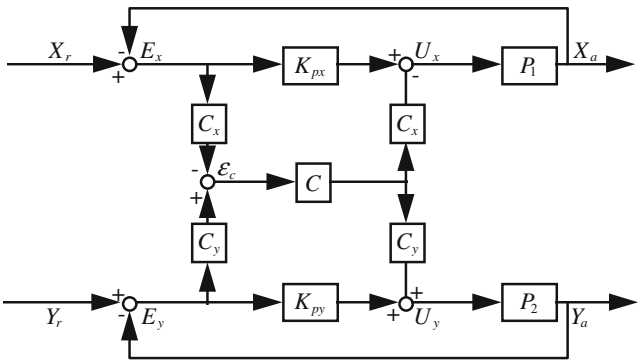

Fig. 2 Block diagram of the coupled motion-control system

By examining Eqs. 11 and 12, the relationship between the contouring error and the coupled and uncoupled systems can be obtained as

$$\varepsilon_c = \frac{1}{1+CK}\varepsilon_o = T \cdot \varepsilon_o \tag{13}$$

where C is the compensator in the CCC to be designed and

$$K = \frac{(1+K_{px}P_1)C_yC_yP_2 + (1+K_{py}P_2)C_xC_xP_1}{(1+K_{px}P_1)(1+K_{py}P_2)} \tag{14}$$

$$T = \frac{1}{1+CK} \tag{15}$$

As represented in Eqs. 13, 14, and 15, the functional relationship T between the coupled and uncoupled motion-control systems is defined as the CETF.

Apparently, the CETF is similar to the sensitivity function in a feedback control system. Therefore, the CETF can be further represented as an equivalent feedback control loop as shown in Fig. 3. Consequently, the design goal of the compensator C in CCC is to reduce the contouring error ε_c and to stabilize the equivalent CCC control system. It should be noted that with the present CETF formulation, various robust algorithms for the controller design can be directly employed to achieve desirable stability margins and performance. Moreover, the design of the compensator C in the present CCC for the two-axis servo system can be simplified to a single-loop design problem as in Fig. 3.

2.3 Design of the DDOB

In real applications, a model-based control design causes the degradation of control performance because of the unavoidable modeling errors and external disturbances.

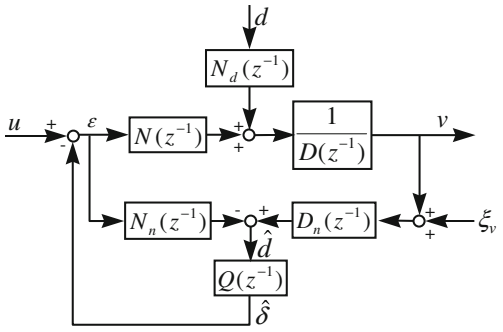

Fig. 4 Structure of the DDOB

Therefore, modeling error reduction and disturbance rejection are usually required for high-precision motion control systems. In this paper, the DDOB [14] is applied to reduce the adverse effects caused by uncertainties, modeling errors, and external disturbances. Figure 4 shows the structure of the DDOB.

By considering the measurement noise ξ_v, the velocity response of the DDOB is derived as

$$v = \frac{N}{D(1-N_nQ)+ND_nQ}u + \frac{N_d(1-N_nQ)}{D(1-N_nQ)+ND_nQ}d - \frac{NQD_n}{D(1-N_nQ)+ND_nQ}\xi_v$$
$$= \frac{N}{D}\frac{1}{(1-N_nQ)+\frac{N}{D}D_nQ}u + \frac{N_d}{D}\frac{(1-N_nQ)}{(1-N_nQ)+\frac{N}{D}D_nQ}d - \frac{N}{D}\frac{D_nQ}{(1-N_nQ)+\frac{N}{D}D_nQ}\xi_v$$

If the filter Q is designed such that $N_n(z^{-1})Q(z^{-1}) = 1$, then

$$v = \frac{N_n}{D_n}u - \xi_v$$

However, if the filter Q is designed such that $N_n(z^{-1})Q(z^{-1}) = 0$, then

$$v = \frac{N}{D}u + \frac{N_d}{D}d$$

Therefore, Q must be designed such that

$$\begin{cases} N_n(z^{-1})Q(z^{-1}) = 1, \text{in the lower frequency region} \\ N_n(z^{-1})Q(z^{-1}) = 0, \text{in the higher frequency region} \end{cases} \quad (16)$$

to degrade the external disturbances and reject the measurement noise. Since the design of Q closely relates to the nominal numerator $N_n(z^{-1})$, the design of Q consists of three steps. First, the stable pole-zero cancellations are directly employed to the filter design. Second, an all-pass filter is employed to reshape the frequency response. Subsequently, a low-pass filter is embedded to achieve the frequency response as in Eq. 16.

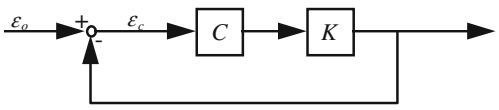

Fig. 3 Equivalent CCC control system

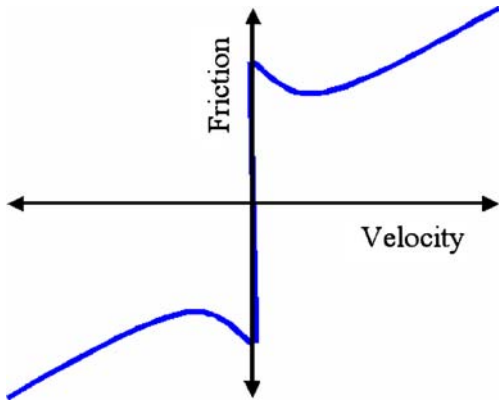

Fig. 5 Nonlinear frictional model [16]

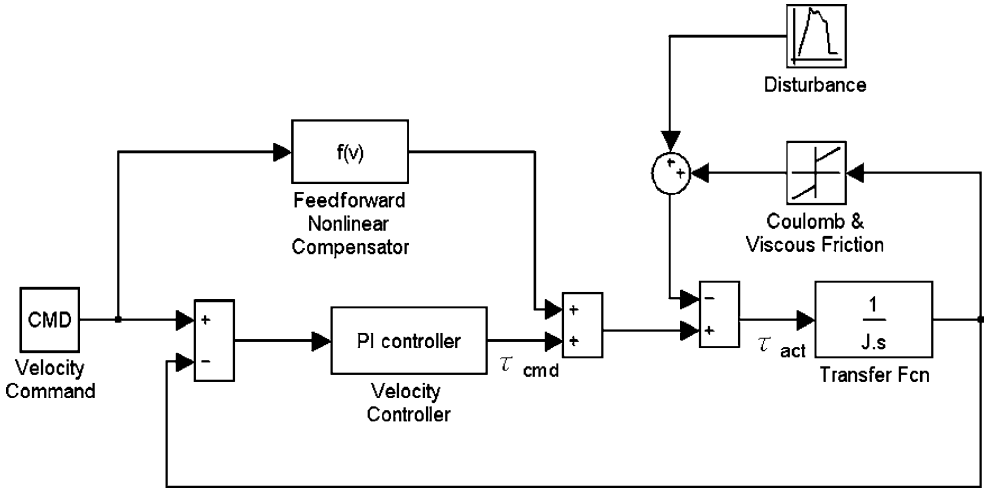

Fig. 6 Velocity loop in motor control

By separating the nominal numerator $N_n(z^{-1})$ as

$$N_n(z^{-1}) = N_n^{\mathrm{a}}(z^{-1})N_n^{\mathrm{u}}(z^{-1})$$

where

$N_n^{\mathrm{a}}(z^{-1})$ is the acceptable polynomial with stable roots and

$N_n^{\mathrm{u}}(z^{-1})$ is the unacceptable polynomial with unstable and nearly unstable roots.

Suppose the unacceptable polynomial $N_n^{\mathrm{u}}(z^{-1})$ is represented as

$$\begin{aligned} N_n^{\mathrm{u}}(z^{-1}) &= b_1 z^{-1} + b_2 z^{-2} + \cdots b_m z^{-m} \\ &= z^{-m}\left(b_1 z^{m-1} + b_2 z^{m-2} + \cdots b_m\right) = z^{-m}\cdot \hat{N}_n^{\mathrm{u}}(z) \end{aligned}$$

Then, Q is designed as

$$Q(z^{-1}) = \frac{1}{N_n^{\mathrm{a}}(z^{-1})\cdot\left[\hat{N}_n^{\mathrm{u}}(z)\right]^*}\cdot \mathrm{LPF}(z^{-1}) \tag{17}$$

where $[\bullet]^*$ denotes the complex conjugate operator and

$$\left[\hat{N}_n^{\mathrm{u}}(z)\right]^* = \left(b_1 z^{-(m-1)} + b_2 z^{-(m-2)} + \cdots b_m\right) \tag{18}$$

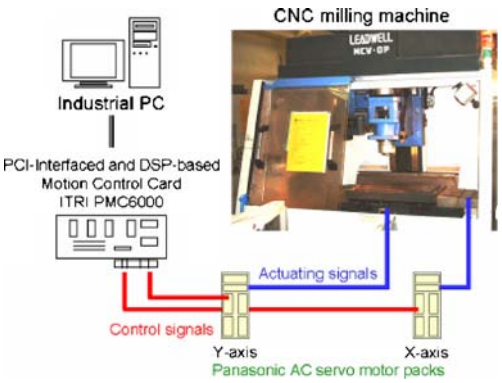

Fig. 7 Experimental setup

It should be noted that Eq. 18 is stable and realizable, and $\frac{N_n^{\mathrm{u}}(z^{-1})}{\left[\hat{N}_n^{\mathrm{u}}(z)\right]^*}$ forms a stable all-pass filter. The low-pass filter $\mathrm{LPF}(z^{-1})$ is designed such that

$$Q(z^{-1})\cdot N_n(z^{-1}) = \frac{N_n^{\mathrm{u}}(z^{-1})}{\left[\hat{N}_n^{\mathrm{u}}(z)\right]^*}\cdot \mathrm{LPF}(z^{-1})$$

achieves the desired frequency response as in Eq. 16.

3 The nonlinear friction compensator

Although the three different linear control algorithms mentioned above can effectively improve the motion precision with regard to the tracking, contouring, and disturbance effects, respectively, they cannot be effectively applied to reduce the nonlinear adverse effects due to friction. In this section, a practical method for friction identification and compensation in CNC machine tools will be introduced.

3.1 Identification of the friction model

In friction compensation, the popular approach is to develop a nonlinear friction model to imitate the relationship between the velocity and friction force/torque as shown in Fig. 5.

The general motor control block used in CNC servo systems is shown in Fig. 6. The torque generated by the servo motors is reduced by the friction and external disturbances when driving the feed tables in real applications. Thus, the torque command is different from the actual torque delivered by the servo motors. Before applying friction compensation, the torque command τ_{cmd} is obtained from the velocity command through the controller in the velocity loop. The actual torque generated by the motor is τ_{act} and $\tau_{\mathrm{act}} = \tau_{\mathrm{cmd}} - \tau_{\mathrm{friction}} - \tau_{\mathrm{disturbance}}$. τ_{friction} and $\tau_{\mathrm{disturbance}}$ are the torques induced by the friction and disturbance effects,

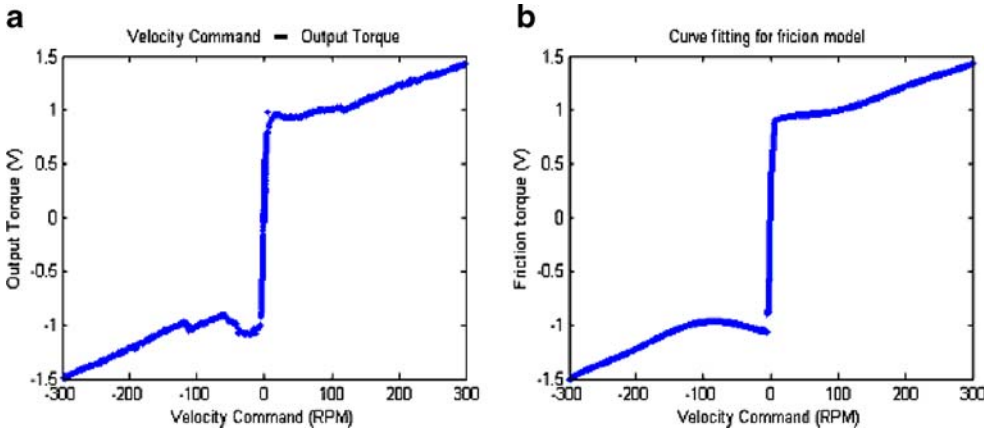

Fig. 8 Velocity and friction torque: **a** experiment and **b** modeling

respectively. Thus, the dynamic motion of machine tools is obtained as follows:

$$J\frac{\mathrm{d}\omega}{\mathrm{d}t} = \tau_{\mathrm{act}} = \tau_{\mathrm{cmd}} - \tau_{\mathrm{friction}} - \tau_{\mathrm{disturbance}} \tag{19}$$

where J is the equivalent inertia of the servo mechanism and ω is the corresponding motor speed. Assuming that the disturbance term $\tau_{\mathrm{disturbance}}$ is compensated by the DDOB and the motion system operates in a steady state, the induced friction torque τ_{friction} can then be suitably obtained by τ_{cmd} as shown in Eq. 19. Therefore, the approach to identify the nonlinear friction effects τ_{friction} is obtained by applying different velocity commands and measuring the corresponding motor current at a steady state to construct the relationship between them.

3.2 Friction compensation

It should be noted that the dominant factors in the friction model are the Coulomb friction at low speeds and the viscous friction at high speeds. The obtained friction model can be divided into multiple segments. Least square curve

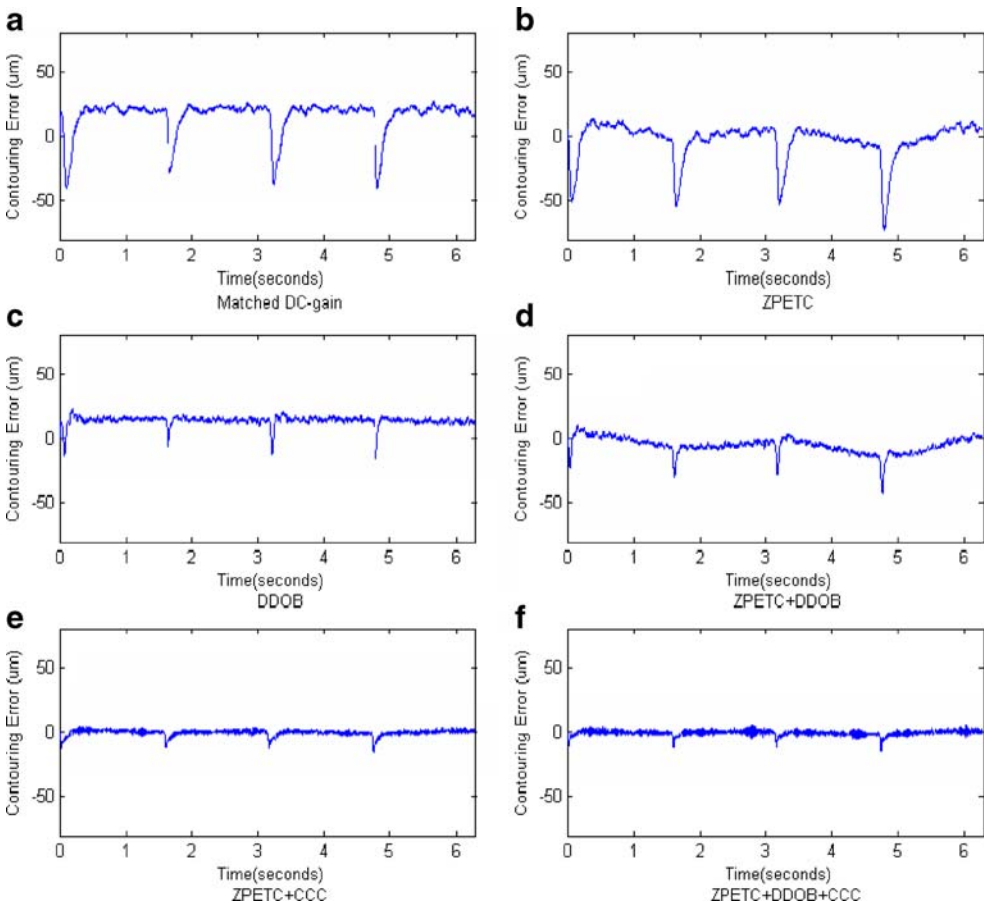

Fig. 9 Contouring error at the command F3000 R50 under different linear controllers

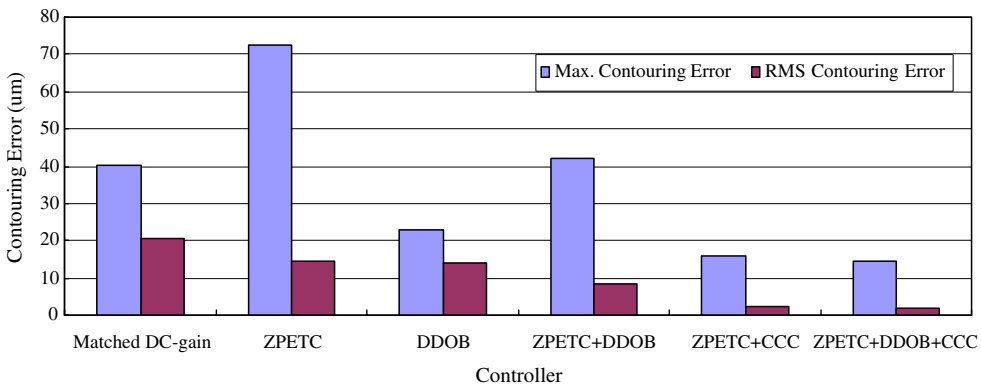

Fig. 10 Contouring error of different linear controllers

fitting is applied to each segment to obtain suitable parameters for the model. In the low-speed region, a higher order model is used because of the discontinuity due to static friction. In the high-speed region, lower order models are used because the curve is more linear.

4 Experimental results and discussion

The experimental setup is applied to a Leadwell MCV-OP CNC milling machine with three-phase Panasonic AC servo motor packs as shown in Fig. 7. The experimental setup mainly consists of an industrial PC and an ITRI PMC6000 DSP-based motion control card. An industrial PC with a Pentium IV 2.8 GHz CPU is used to provide functions including an interface for human and machine operations, an interpreter for interpreting standard NC codes, and recording signals during motions. The DSP-based motion control card with a high-performance TI TMS320C32 DSP is used to implement the present motion controllers for controlling the AC servo motor packs with a sampling period of 1.0 ms.

Since circular contours are usually applied to test the motion control system of a commercialized CNC milling

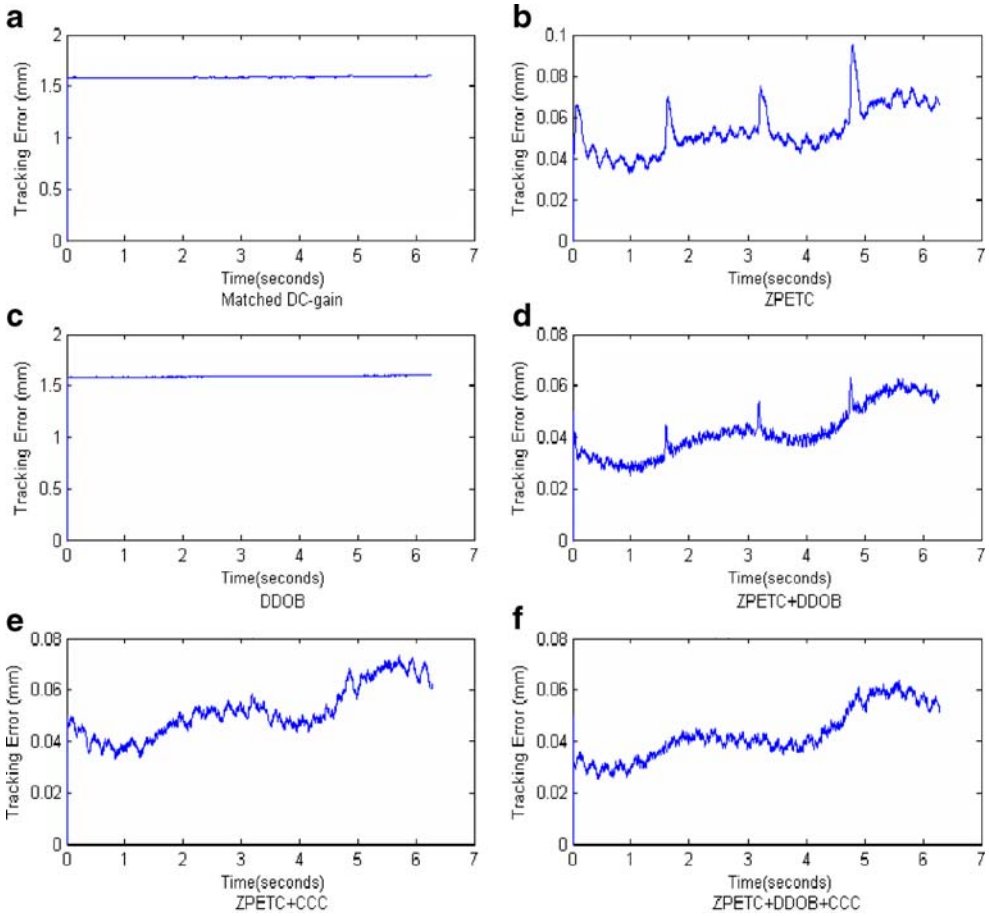

Fig. 11 Tracking error at the command F3000 R50 under different linear controllers

machine, circular contours with different radii and motion speeds are applied to evaluate the motion performances of the different motion controllers in this study. Moreover, two important performance indices, the maximum (Max) value and root-mean-square (RMS) value of the tracking and contouring errors, are used to evaluate motion performances. The motion performances measured by the DBB are further employed to evaluate the motions of the CNC milling machine using different motion controllers.

4.1 Design of linear controllers

For designing linear controllers by applying the ARX modeling processes, the velocity models of each axis can be obtained as

$$V_x(z^{-1}) = \frac{0.174324z^{-3} + 0.055299z^{-4} + 0.018861z^{-5} + 0.032584z^{-6}}{[1 - 0.33354z^{-1} - 0.26079z^{-2} - 0.19207z^{-3} - 0.065409z^{-4} + 0.002068z^{-5} + 0.007182z^{-6} + 0.124797z^{-7}]}$$

$$V_y(z^{-1}) = \frac{0.186132z^{-3} + 0.028259z^{-4}}{[1 - 0.391058z^{-1} - 0.363857z^{-2} - 0.115917z^{-3} + 0.033927z^{-4} + 0.004945z^{-5} - 0.06318z^{-6} - 0.00116z^{-7} + 0.111347z^{-8}]}$$

Moreover, since all the axes must be stable and present in similar DC gains for improving the contouring accuracy, we designed suitable gains for the position loop controllers as K_{px}=0.035 and K_{py}=0.035; therefore, their position loop transfer functions with matched DC gain are obtained as

$$P_x(z^{-1}) = \frac{0.00477z^{-1}}{1 - 1.70318z^{-1} + 0.17889z^{-2} + 0.490335z^{-3} + 0.3870008z^{-4} - 0.350434z^{-5}}$$

$$P_y(z^{-1}) = \frac{0.0025132z^{-3}}{1 - 1.733067z^{-1} + 0.2450446z^{-2} + 0.528681z^{-3} + 0.2276909z^{-4} - 0.265799z^{-5}}$$

The design results of the ZPETC and DDOB are directly obtained as

ZPETC:

$$Z_x(z^{-1}) = 382.78835z^3 - 651.9575z^2 + 68.477303z + 187.69478 \quad + 148.13942z^{-1} - 134.1423z^{-2}$$

$$Z_y(z^{-1}) = 392.10965z^3 - 679.5523z^2 + 96.08437z + 207.30116 \quad + 89.2798z^{-1} - 104.2226z^{-2}$$

DDOB:

$$Q_x(z^{-1}) = \frac{\mathrm{LPF}(z^{-1})}{1 + 0.317224z^{-1} + 0.108198z^{-2} + 0.1869207z^{-3}}$$

$$Q_y(z^{-1}) = \frac{\mathrm{LPF}(z^{-1})}{1 + 0.1518257z^{-1}}$$

By selecting the cut-off frequency of a third-order IIR low-pass filter LPF(z^{-1}) as 30 Hz, the transfer function is obtained as follows:

$$\mathrm{LPF}(z^{-1}) = \frac{0.00069934 + 0.002098z^{-1} + 0.002098z^{-2} + 0.00069934z^{-3}}{1 - 2.6235518z^{-1} + 2.314682z^{-2} - 0.6855359z^{-3}}$$

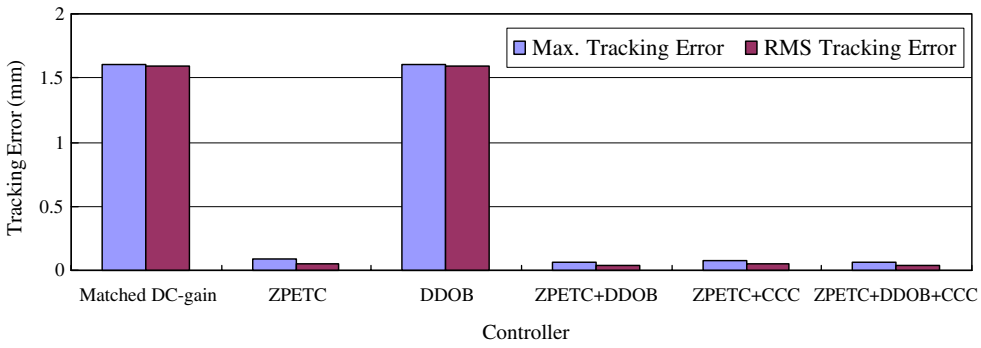

Fig. 12 Tracking error of different linear controllers

In the CCC design, a proper constant gain is set as C=1.3.

4.2 Design of the nonlinear friction compensator

In the design of nonlinear compensators by applying different velocity commands to each axis from 0 to ±300 rpm and recording the corresponding motor current at a steady state, the friction effects can be obtained as shown in Fig. 8a. Figure 8b shows the curve-fitting results.

The friction model corresponding to five speed ranges for the two motion axes are obtained as follows:
X-axis:

$$\tau(v)=\begin{cases} 0.73838718+0.0018525v, v\ >300\ \text{rpm} \\ 0.65+0.0063v-5.9\times10^{-5}v^2+3.09\times10^{-7}v^3 \\ -6.7\times10^{-10}v^4+4.7\times10^{-13}v^5,\ 5<v\leqq300\ \text{rpm} \\ 0.13+0.24v-0.026v^2-0.0095v^3 \\ +0.000887v^4+0.000216v^5,\ -5\leqq v\leqq5\text{rpm} \\ -0.83-0.00126v-7.45\times10^{-5}v^2-6.96\times10^{-7}v^3 \\ -2.65\times10^{-9}v^4-3.53\times10^{-12}v^5, -5>v\geqq-300\ \text{rpm} \\ -0.7103+0.0020742v, v\ <\ -300\ \text{rpm} \end{cases}$$

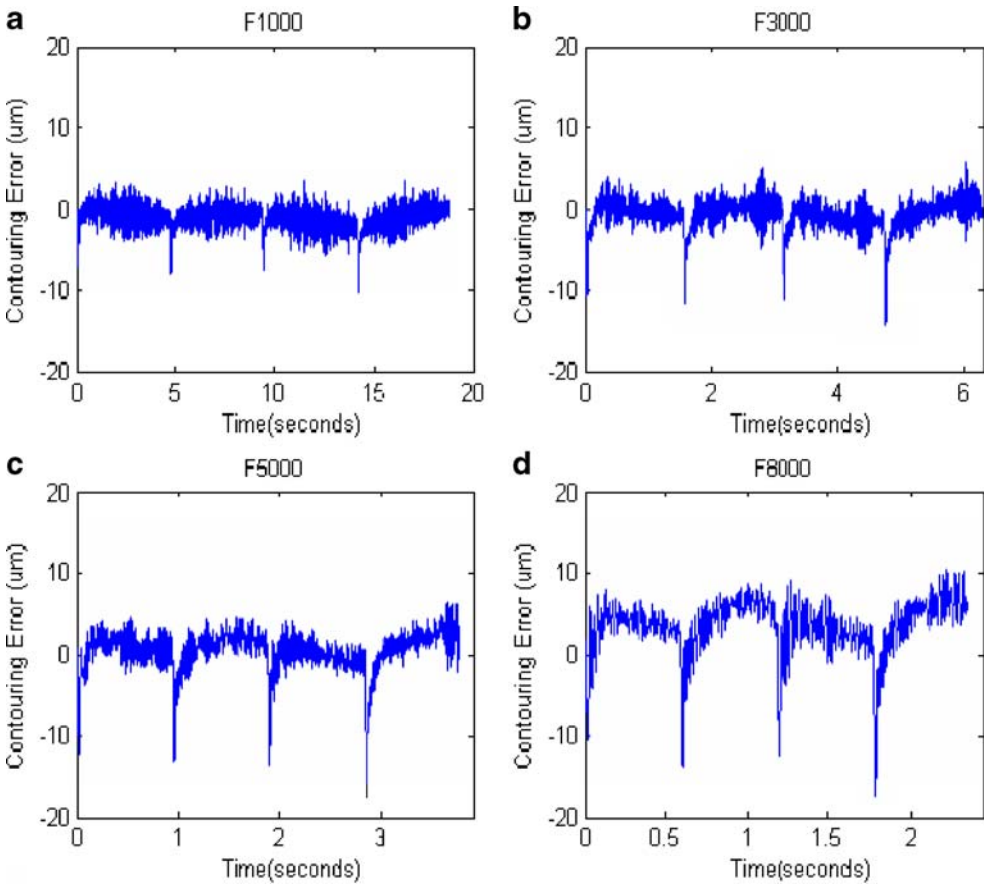

Fig. 13 Contouring error of the linear controller without a nonlinear compensator under different feed rates

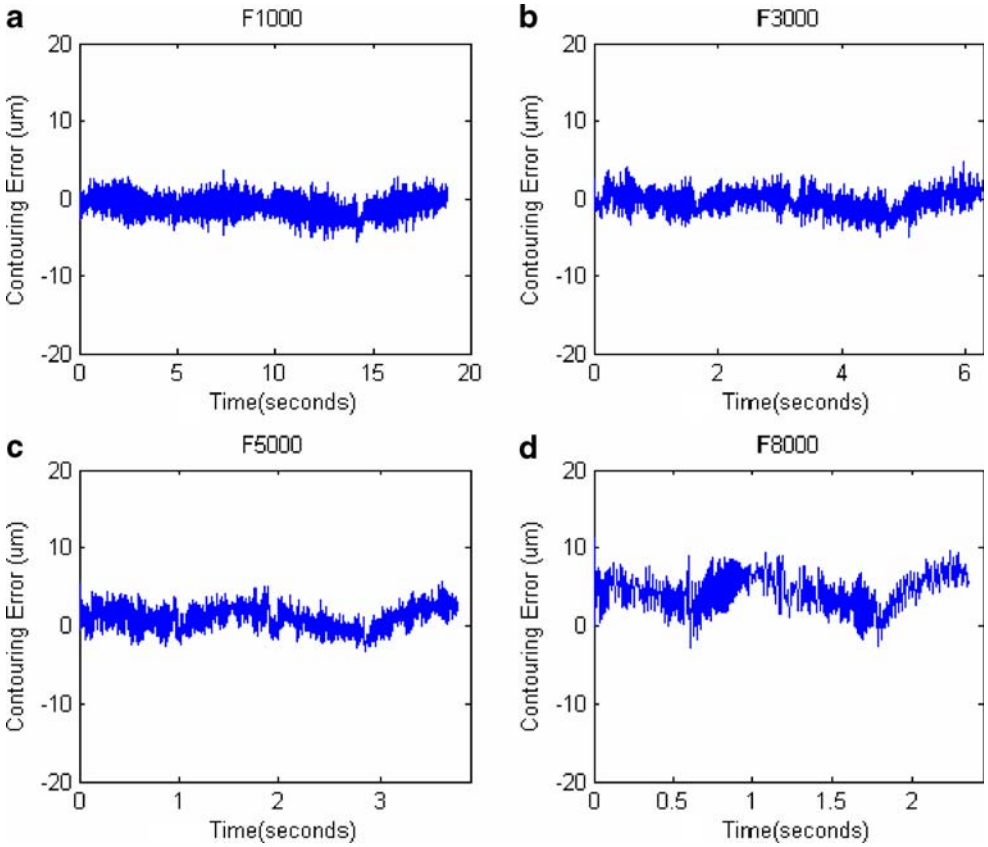

Fig. 14 Contouring error with nonlinear compensation under different feed rates

Y-axis:

$$\tau(v) = \begin{cases} 0.8677 + 0.00118v\,, v > 300\,\text{RPM} \\ 0.63 + 0.011v - 0.00015v^2 + 1.07 \times 10^{-6}v^3 \\ -3.37 \times 10^{-9}v^4 + 3.95v^5,\ 5 < v \leqq 300\ \text{rpm} \\ 0.141 + 0.291v - 0.0289v^2 - 0.0134v^3 \\ + 0.00097v^4 + 0.000287v^5,\ -5 \leqq v \leqq 5\ \text{rpm} \\ -0.7524 + 0.0021v + 5.91 \times 10^{-6}v^2 + 2.56 \times 10^{-8}v^3 \\ + 6.42 \times 10^{-11}v^4 + 6.56 \times 10^{-14}v^5,\ -5 > v \geqq -300\ \text{rpm} \\ -0.819 + 0.00128\text{v},\ v - 300\ \text{rpm} \end{cases}$$

4.3 Experimental results of the linear controllers

To compare the performances of the motion system with different linear controllers, circular commands were provided with a radius of 50 mm under a feed rate of 3,000 mm/min. Figures 9 and 10 show the contouring performances, while Figs. 11 and 12 show the tracking performances of the motion system with different linear controllers. For the performances obtained using only the DC-gain-matched position feedback controllers, the maximum contouring error is approximately 40 μm, and the tracking error is quite large because of the servo lags of the motion systems. After applying the ZPETC, the tracking error is significantly reduced, but the contouring accuracy is still limited because of the modeling uncertainties and nonlinear external disturbances such as friction effects. When the DDOB is added to the motion system, as shown in Fig. 9c, d, the adverse effects caused by the modeling uncertainties and friction phenomena are significantly reduced, and the maximum contouring error is reduced by approximately 50%. Although

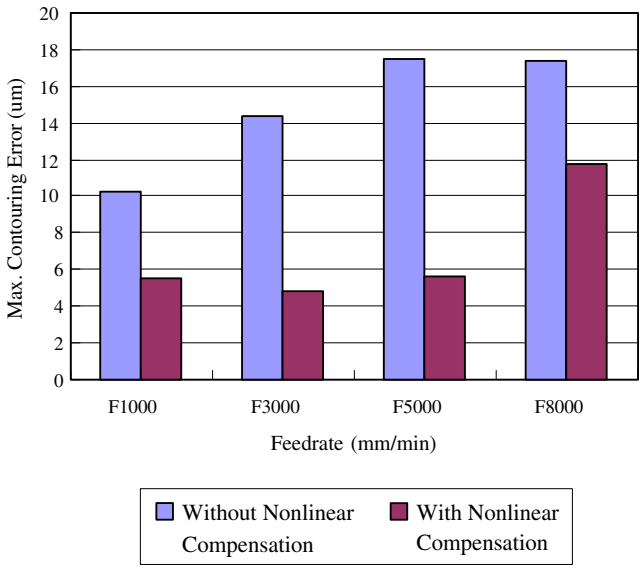

Fig. 15 Summary of Figs. 12 and 13 with regard to the maximum contouring error

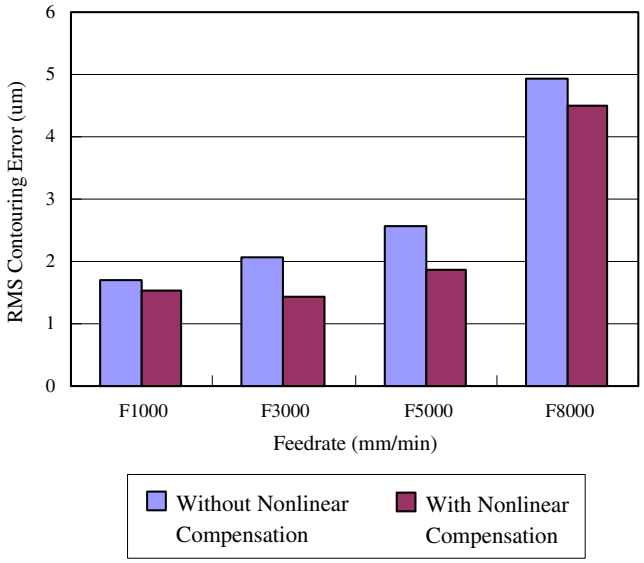

Fig. 16 Summary of Figs. 12 and 13 with regard to the RMS contouring error

nonlinear phenomena due to friction effects cannot be completely eliminated, the motion control system with both the ZPETC and CCC can significantly reduce both the tracking and the contouring errors. The maximum contouring error is reduced to approximately 16 μm, while the maximum tracking error is reduced to approximately 60 μm. Figures 10 and 12 summarize the comparison between the different linear controllers by considering the maximum and the RMS errors in contouring and tracking errors, respectively. Apparently, the RMS errors are significantly diminished when the motion control system uses the DDOB, ZPETC, and CCC. From these figures, we conclude that the motion system with the ZPETC can significantly improve the tracking accuracy, and the maximum tracking error is reduced to 1/17th of the motion control system without using the ZPETC. Moreover, the contouring accuracy is improved by applying both the CCC and the DDOB. The integrated linear controller that comprises the DDOB, ZPETC, and CCC reduces both the tracking and contouring errors. However, since the nonlinear friction effects still influence the motion system, and these performances are still limited, the nonlinear compensation is required for improving the motion accuracy.

4.4 Experimental results of the nonlinear compensator

In this study, four circular commands with an identical radius of 50 mm but with different feed rates were applied for testing the performances of the proposed control structure under different motion speeds. The applied feed rates are 1,000, 3,000, 5,000, and 8,000 mm/min. When the motion system only incorporates the integrated linear controller that comprises the DDOB, ZPETC, and CCC, as shown in Fig. 13, the maximum contouring error increases depending on the motion speed, and it is dominated by the friction phenomena. By applying the proposed nonlinear compensators, as shown in Fig. 14, the contouring errors are significantly reduced for all the motion

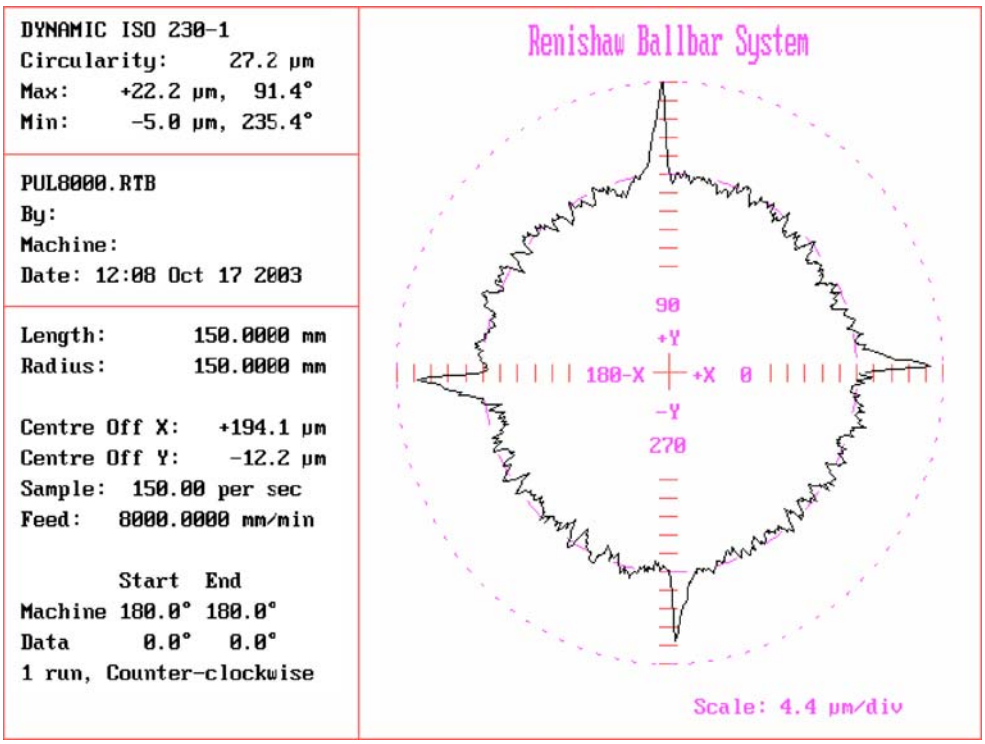

Fig. 17 Contouring error in the DBB measurement when applying the existing controller

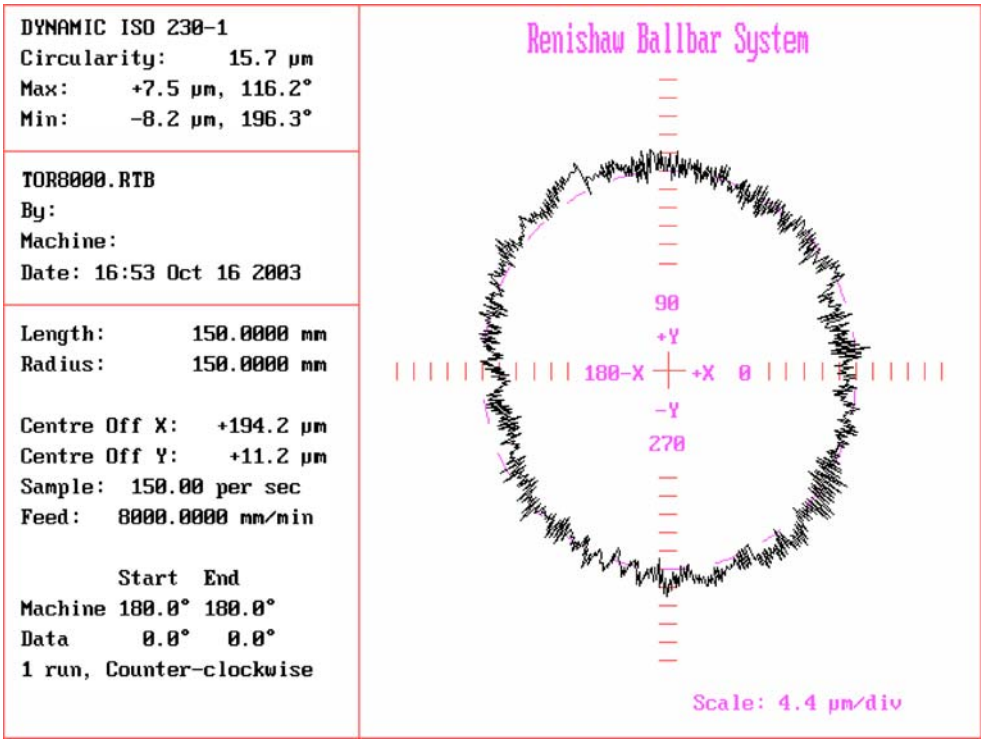

Fig. 18 Contouring error in the DBB measurement for applying the proposed control structure

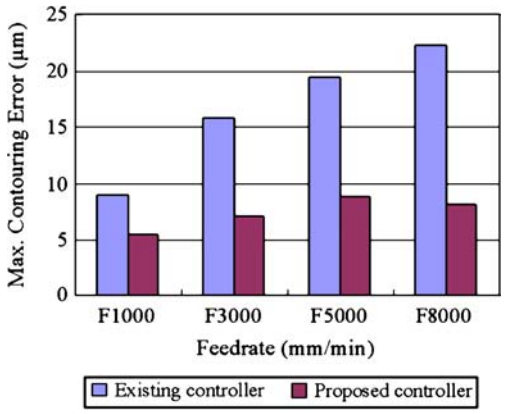

Fig. 19 Comparison of the maximum contouring errors

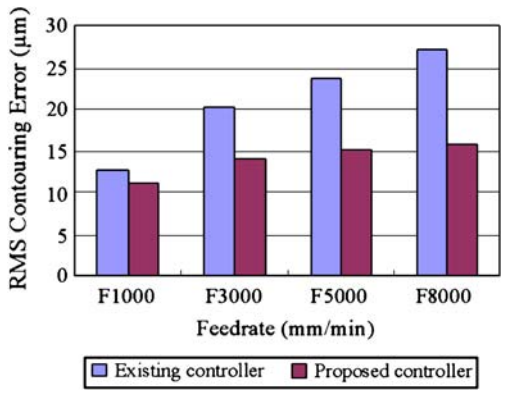

Fig. 20 Comparison of the RMS contouring errors

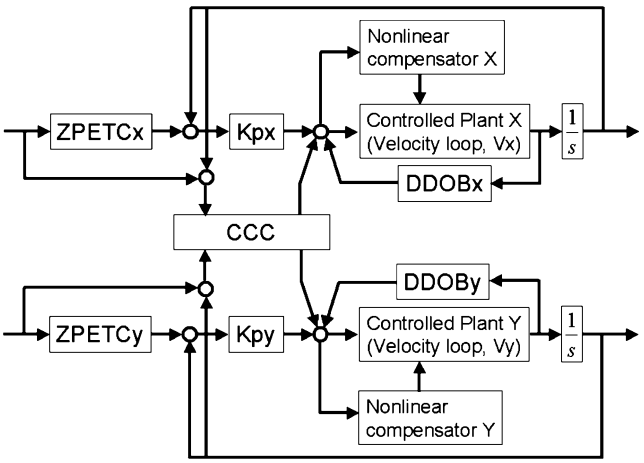

Fig. 21 Sketch block diagram of the proposed integrated controller

Table 1 Summary of experimental results

Controller	Performance		
	Tracking accuracy	Contouring accuracy	Friction elimination
ZPETC			
CCC		••	
DDOB		•	•
Nonlinear compensation			••
The integrated motion control structure	••	••	••

• improvement; •• significant improvement

speeds. Figures 15 and 16 summarize the comparison between the different control structures with different motion speeds by considering the maximum and the RMS contouring errors. Apparently, the experimental results indicate that the motion control system with the proposed nonlinear compensators can achieve considerably better operating performances.

4.5 DBB measurement

We also compared the proposed control structure with the existing commercialized control structure using the DBB circular measurement equipment. The circular commands with an identical radius of 150 mm but with different feed rates were provided for testing the performances, and the corresponding contouring errors are measured using the DBB measurement system. The applied feed rates are 1,000, 3,000, 5,000, and 8,000 mm/min. Figure 17 shows the measuring results under a feed rate of 8,000 mm/min when the motion system uses the existing control structure. Figure 17 shows that the friction phenomena significantly affect the operating performances before applying the proposed nonlinear compensation. The maximum contouring error mainly induced by the friction effects is 22.2 μm. Figure 18 shows the measurement results when the motion system uses the proposed control structure. The experimental results indicate that the friction phenomena are successfully suppressed, and the maximum contouring error is 8.2 μm. The maximum contouring error is reduced by approximately 60%. Figures 19 and 20 summarize the comparison between the different control structures with different motion speed by considering the maximum and the RMS contouring errors, respectively. Apparently, both the Max and RMS contouring errors of the motion system with the existing control structure substantially increase with the feed rate. However, for the motion system with the proposed control structure, both the maximum and RMS contouring errors increase only slightly. This result also shows the robustness of the proposed control structure.

5 Conclusion

In this paper, we have studied the integrated motion control structure, as shown in Fig. 21, which consists of three linear controllers, ZPETC, CCC, and DDOB, and one nonlinear compensator for improving the motion accuracy of industrial CNC machines. Moreover, the integrated control structure has been successfully applied to a CNC vertical machining center, and the experimental results show that the control structure can improve both the tracking and contouring accuracies and reduce the adverse effects caused by modeling uncertainties and external disturbances such as friction effects. In comparison with the existing commercialized control structure, the integrated motion control structure achieves both motion precision and robustness. All the experimental results are summarized, as shown in Table 1, to indicate the merits of applying the integrated motion control to CNC machines.

Acknowledgment This work was supported by National Science Council of the Republic of China under Contract NSC 95-2218-E-027-026, NSC 91-2212-E-009-035, and Industrial Technology Research Institute under contract no. C92054. The authors would like to thank Mr. Jin-Tsu Sun and Mr. Mao-Feng Tu at the Mechanical and Systems Laboratories of Industrial Technology Research Institute for their assistance and valuable comments.

References

1. Koren Y, Lo CC (1991) Variable gain cross coupling controller for contouring. Ann CIRP 40:371–374. doi:10.1016/S0007-8506(07)62009-5
2. Clarke DW (1984) Self tuning control of non-minimum phase systems. Automatica 20:501–517. doi:10.1016/0005-1098(84)90003-7
3. Tomizuka M (1987) Zero phase error tracking algorithm for digital control. ASME J Dyn Syst Meas Contr 109:65–68
4. Hsu PL, Houng YC (1996) An integrated controller design for precise CNC motion control. Ann CIRP 25(1):91–96
5. Yeh SS, Hsu PL (2002) Estimation of the contouring error vector for the cross-coupled control design. IEEE/ASME Trans Mechatron 7(1):44–51. doi:10.1109/3516.990886
6. Shih YT, Chen CS, Lee AC (2002) A novel cross-coupling control design for Bi-axis motion. Int J Mach Tools Manuf 42(14):1539–1548. doi:10.1016/S0890-6955(02)00109-8
7. Chen SL, Liu HL, Ting SC (2002) Contouring control of biaxial systems based on polar coordinates. IEEE/ASME Trans Mechatron 7(3):329–345. doi:10.1109/TMECH.2002.802723
8. Lo CC (1998) Three-axis contouring control based on a trajectory coordinate basis. JSME Int J Ser C Mech Syst Mach Elem Manuf 41(2):242–247
9. Chiu GTC, Tomizuka M (2001) Contouring control of machine tool feed drive systems: a task coordinate frame approach. IEEE Trans Contr Syst Technol 9(1):130–139. doi:10.1109/87.896754
10. Yeh SS, Hsu PL (1999) Theory and applications of the robust cross-coupled control design. ASME Trans Dyn Syst Meas Contr 121(3):524–530. doi:10.1115/1.2802506
11. Chen CS, Fan YH, Tseng SP (2006) Position command shaping control in a retrofitted milling machine. Int J Mach Tools Manuf 46(3-4):293–303. doi:10.1016/j.ijmachtools.2005.05.018
12. Ohishi K, Nakao M, Ohnishi K, Miyachi K (1985) Microprocessor-controlled DC motor for load-insensitive position servo system. IEEE Trans Ind Electron IE 34(1):44–49. doi:10.1109/TIE.1987.350923
13. Umeno T, Hori Y (1991) Robust speed control of dc servomotors using modern two degree-of-freedom controller design. IEEE Trans Ind Electron 38(5):363–368. doi:10.1109/41.97556
14. Yeh SS, Hsu PL (2004) Perfectly matched feedback control and its integrated design for multi-axis motion systems. ASME J Dyn Syst Meas Contr 126(3):547–557. doi:10.1115/1.1789970
15. Yan MT, Huang KY, Shiu YJ, Chen Y (2007) Disturbance observer and adaptive controller design for a linear-motor-driven table system. Int J Adv Manuf Technol 35(3-4):408–415. doi:10.1007/s00170-007-1173-y

16. Mei X, Tsutsumi M, Tao T, Sun N (2004) Study on the compensation of error by stick-slip for high-precision table. Int J Mach Tools Manuf 44(5):503–510. doi:10.1016/j.ijmachtools.2003.10.027
17. Mei ZQ, Xue YC, Yang RQ (2006) Nonlinear friction compensation in mechatronic servo systems. Int J Adv Manuf Technol 30 (7–8):693–699. doi:10.1007/s00170-005-0113-y
18. Johnson CT, Lorenz RD (1992) Experimental identification of friction and its compensation in precise, position controlled mechanisms. IEEE Trans Ind Appl 28(6):1392–1398. doi:10.1109/28.175293
19. Chen JS, Kuo YH, Hsu WY (2006) The influence of friction on contouring accuracy of a Cartesian guided tripod machine tool. Int J Adv Manuf Technol 30(5-6):470–478. doi:10.1007/s00170-005-0088-8
20. Armstrong-Helouvry B, Pierre D, Canudas DWC (1994) A survey of models, analysis tools and compensation methods for the control of machines with friction. Automatica 30(7):1083–1138. doi:10.1016/0005-1098(94)90209-7